Nuclear Magnetic Resonance Solution Structure of the Plasminogen-Activator Protein Staphylokinase[†,‡]

Oliver Ohlenschläger,[§] Ramadurai Ramachandran,[§] Karl-Heinz Gührs,[||] Bernhard Schlott,[||] and Larry R. Brown*[,§]

Department of Molecular Biophysics and NMR Spectroscopy and Department of Biochemistry, Institute for Molecular Biotechnology, Postfach 100813, D-07708 Jena, Germany

Received March 23, 1998; Revised Manuscript Received May 8, 1998

ABSTRACT: Staphylokinase, a 15.5 kDa protein from *Staphylococcus aureus*, is a plasminogen activator which is currently undergoing clinical trials for the therapy of myocardial infarction and peripheral thrombosis. The three-dimensional (3D) NMR solution structure has been determined by multidimensional heteronuclear NMR spectroscopy on uniformly ^{15}N- and ^{15}N,^{13}C-labeled samples of staphylokinase. Structural constraints were obtained from 82 $^{3}J_{\mathrm{HNH}\alpha}$ as well as 22 $^{3}J_{\mathrm{NH}\beta}$ scalar coupling constants and 2345 NOE cross-peaks, derived from ^{15}N-edited and ^{13}C-edited 3D NOE spectra. NOE cross-peak assignments were confirmed by analysis of {^{15}N,^{13}C}-edited and {^{13}C,^{13}C}-edited 4D NOE spectra. The structure is presented as a family of 20 conformers which show an average rmsd of 1.02 ± 0.15 Å from the mean structure for the backbone atoms. The tertiary structure of staphylokinase shows a well-defined global structure consisting of a central 13-residue α-helix flanked by a two-stranded β-sheet, both of which are located above a five-stranded β-sheet. Two of the connecting loops exhibit a higher conformational heterogeneity. Overall, staphylokinase shows a strong asymmetry of hydrophilic and hydrophobic surfaces. The N-terminal sequence, including Lys10 which is the site of the initial proteolytic cleavage during activation of plasminogen, folds back onto the protein core, thereby shielding amino acids with functional importance in the plasminogen activation process. From a comparison of the structure with mutational studies, a binding region for plasminogen is proposed.

The bacterial protein staphylokinase (Sak)[1] is potentially useful for the therapy of myocardial infarction (*1*, *2*) or peripheral thrombosis (*3*) since it is capable of activating the mammalian plasma protein plasminogen. Plasmin, the protease formed by activation of plasminogen, degrades fibrin clots. Since plasmin cannot activate plasminogen in an autocatalytic pathway and Sak has no inherent proteolytic activity, the active species is thought to be a plasmin(ogen)−Sak complex (*2*, *4*). Thus, the activation mechanism of staphylokinase resembles that of streptokinase (*5*) in that a protein−protein complex with altered proteolytic specificity is the active species. This is different from tissue plasminogen activator and urokinase, which activate plasminogen by their inherent proteolytic activity (*6*, *7*). The Sak−plasmin(ogen) complex shows a high degree of specificity for cleavage of clots with reduced side effects because, in contrast to streptokinase activation, the Sak−plasmin(ogen) complex is strongly inhibited by α2-antiplasmin circulating in the blood (*2*, *8*, *9*). The cleavage of the Lys10−Lys11 peptide bond of Sak in the Sak−plasmin(ogen) complex, presumably by plasmin, is a prerequisite for the formation of a species capable of activating plasminogen and ultimately is the trigger of the fibrin specificity of Sak (*10*). The apparent ability of Sak to change the proteolytic specificity of plasmin(ogen) presumably results from three-dimensional (3D) conformational changes in the Sak−plasmin(ogen) complex.

The 3D structure of staphylokinase may serve as a starting point for understanding the mechanisms by which Sak can alter the proteolytic specificity of plasmin and hence for the design of improved drugs for lysis of blood clots. We are currently investigating the conformations of native and mutant staphylokinases. In a recent report, we identified the elements of the secondary structure of Sak residues 1−136 in solution by heteronuclear NMR spectroscopy (*11*). The secondary structural elements observed in the solution structure showed slight but potentially important differences with respect to the recently published X-ray structure of Sak residues 10−136 (*12*), i.e., the molecular species produced by the first step in the activation of plasminogen. In this paper, we report the 3D solution structure of the full-length Sak molecule and this structure is discussed in the context of biochemical and mutational data on the mechanism of activation of plasminogen by staphylokinase.

MATERIALS AND METHODS

NMR Sample Preparation. The NMR samples of recombinant staphylokinase SakSTAR were expressed in *Escherichia coli* TG1 transformed with plasmid pMEX602sakB and purified as recently described (*11*, *13*). The concentrations of the SakSTAR samples were 1.1 ([^{15}N]SakSTAR) and 1.28 mM ([^{13}C,^{15}N]SakSTAR). A sample of staphylokinase in

[†] This work has been supported by the Fonds der Chemischen Industrie.

[‡] Coordinates have been deposited in the Brookhaven Protein Data Bank under file name 1SSN.

* To whom correspondence should be addressed.

[§] Department of Molecular Biophysics and NMR Spectroscopy.

[||] Department of Biochemistry.

[1] Abbreviations: AOP, angular order parameter; rmsd, root-mean-square deviation; Sak, staphylokinase.

S0006-2960(98)00673-4 CCC: $15.00
Published on Web 07/09/1998

D_2O was prepared by passing the Sak sample over a NAP-25 column (Pharmacia, Freiburg, Germany) which was equilibrated with D_2O buffer as described previously (*11*).

NMR Spectroscopy. All NMR spectra were recorded at 300 K on a Varian INOVA 750 MHz four-channel NMR spectrometer equipped with pulse field gradient accessories and a triple-resonance probe with an actively shielded Z gradient coil. The States procedure (*14*) was used for quadrature detection in the indirect dimensions. Water suppression was achieved via the WATERGATE technique (*15*) or by low-power presaturation during the recycle delay. ^{15}N and ^{13}C broad-band decoupling used the GARP (*16*) or MPF7 (*17*) decoupling schemes. Where applicable, isotropic mixing was performed with either the DIPSI-2 or DIPSI-3 sequences (*18*). Multidimensional data sets were analyzed with the program XEASY (*19*) on Silicon Graphics INDY and INDIGO2 workstations. Proton chemical shifts were referenced to the H_2O signal at 4.74 ppm relative to DSS; ^{15}N chemical shifts were referenced to external 2.9 M $^{15}NH_4Cl$ in 1 M HCl at 24.93 ppm relative to liquid ammonia. ^{13}C chemical shifts were referenced to TSP at 0.0 ppm by adding 1.6 ppm to the values initially obtained for external dioxane/H_2O at 67.8 ppm as described previously (*20*). Unless indicated, the ^1H and ^{15}N carriers were set at 4.74 and 119.5 ppm, respectively, and a recycle time of 1 s was normally employed. Other relevant NMR data acquisition parameters are listed in Table 1 of the Supporting Information.

The 3D ^{15}N-edited NOESY−HSQC (*21*, *22*) experiment was carried out employing a mixing time of 50 ms. The 3D ^{13}C-edited NOESY−HSQC experiments in D_2O for the aliphatic and aromatic carbons were carried out separately with a mixing time of 50 ms. The 4D {^{13}C,^{15}N}- and {^{13}C,^{13}C}-edited HMQC−NOESY−HSQC experiments (*23*, *24*) in H_2O and D_2O, respectively, were carried out with a mixing time of 50 ms, using the parameters listed in Table 1 of the Supporting Information. For the latter experiment, the ^{13}C spectral widths and the carrier frequency were chosen to fold the $^{13}C^{\alpha}$ resonances, thereby improving the spectral resolution in the indirect dimensions. When required, carbonyl decoupling was achieved by the SEDUCE-1 pulse scheme (*25*). The resonance assignments reported earlier (*11*) were further extended by analysis of the 3D HCCH−TOCSY data (aliphatic and aromatic regions), 2D $^{13}C-^1H$ HSQC spectra of the aliphatic and aromatic resonances, and 3D ^{13}C-edited NOE data for the aromatic resonances. The resulting resonance assignments are provided in Table 2 of the Supporting Information. The 4D data sets were linearly predicted and processed with the NMR Pipe program of Delaglio et al. (*26*), and the resulting spectral data were converted into XEASY format for further analysis. Three-bond coupling constants $^3J_{HNH\alpha}$ were extracted from the 3D HNHA spectrum (*27*), and $^3J_{NH\beta}$ coupling constants were obtained via the method of Montelione et al. (*28*) by fitting the E.COSY pattern observed in the ^{15}N-edited 3D NOE data with the program SPSCAN (*29*). Heteronuclear $^{15}N-\{^1H\}$ NOE measurements were made using the uniformly ^{15}N-labeled sample according to the sequence of Kay et al. (*30*). The heteronuclear NOEs were calculated by normalization of the difference between the cross-peak integrals in the presence and absence of the $^{15}N-\{^1H\}$ NOE with the integral of the latter.

Structure Calculation. The NOE cross-peak intensities were classified into three categories (strong, medium, and weak) corresponding to inter-hydrogen upper bound distance constraints of 2.7, 3.8, and 5.5 Å, respectively. For residues in the β-sheet and α-helix regions which showed a consistent hydrogen bonding pattern in the first cycle of calculations and which exhibited slow exchange of amide hydrogens with solvent water, additional constraints consisting of a limit of 2.4 Å for the H^N-O distance were introduced in subsequent calculations. No explicit lower bounds were defined; i.e., the atomic van der Waals radii served as lower limits. Torsion angle constraints, calculated from a local conformational analysis employing the NOE intensities together with $^3J_{NH\beta}$ and $^3J_{HNH\alpha}$ coupling constants, were also incorporated. The program DYANA, version 1.4 (*31*), was used for structure calculations. For the restrained simulated annealing calculations in torsion angle space, an ensemble of 100 structures was typically generated with the DYANA protocol. In contrast to the standard protocol, 30 000 steps of torsion angle dynamics and 6000 minimization steps were performed. On the basis of the converged structures obtained in a first calculation, additional NOE assignments were made using the program ASNO (*32*). The restrained energy minimizations of the 20 best conformers were performed with the SANDER module of the program AMBER, version 4.1 (*33*), using the all-atom force field (*34*). The consecutive steepest descent, conjugate gradient minimization was run until the difference in the norm of the gradient was below the threshold of 0.01 kcal mol^{-1} $Å^{-1}$ for successive steps. A distance-dependent dielectric constant was employed (*35*). Distance and torsion angle restraints were incorporated using a flat−parabolic−linear potential function with limits of 0.5 Å and 10° and force constants of 25 kcal mol^{-1} $Å^{-2}$ and 50 kcal mol^{-1} rad^{-2}, respectively. The programs MOLMOL (*36*) and SYBYL (TRIPOS, St. Louis, MO) were used for the visualization of structures and the production of figures. The coordinates of the staphylokinase solution structures have been deposited in the Brookhaven Protein Data Bank.

RESULTS AND DISCUSSION

NMR Resonance Assignments. Using the known chemical shifts of ^{13}C and ^1H resonances for the α- and β-atoms as a starting point (*11*), analysis of the 3D HCCH−TOCSY spectrum allowed virtually complete resonance assignments to be obtained. Ninety-five percent of the hydrogen atoms (H^N 97%, H^{α} 100%, H^{β} 99%, H^{γ} 99%, H^{δ} 98%, H^{ϵ} 100%, and H^{ζ} 75%), 90% of the carbons (C′ 87%, C^{α} 99%, C^{β} 100%, C^{γ} 72%, C^{δ} 80%, C^{ϵ} 90%, and C^{ζ} 24%), and 97% of the backbone nitrogens were assigned. Only eight of the nonlabile hydrogens (H^{β} of His43, H^{γ} and H^{δ} of Lys59, and H^{ζ} of Phe76 and Phe111) and four of the labile amide H^N hydrogens (Ser1, Tyr44, Lys57, and Lys74) could not be identified. Unusually strong deviations from the statistical distributions of amino acid chemical shifts (as implemented in the DYANA library) were observed only for the N atom of Met26 (2.2 ppm) as well as for the γ-carbon of Glu46 (4.7 ppm). To verify NOE assignments, {^{15}N,^{13}C}-edited and {^{13}C,^{13}C}-edited 4D NOESY spectra were acquired in addition to the ^{15}N-edited and ^{13}C-edited 3D NOESY data sets. Figure 1 shows a typical cross section from the {^{15}N,^{13}C}-edited 4D NOESY spectrum used to assign the 3D ^{15}N-edited NOESY spectrum. In the 4D H−C plane

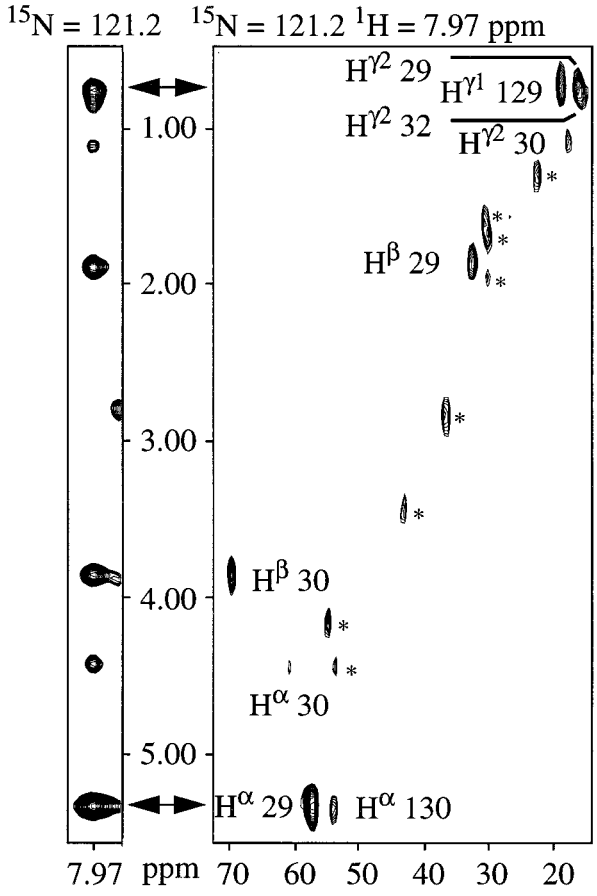

FIGURE 1: (Left) 2D slice of the ^{15}N-edited 3D NOESY−HSQC spectrum. (Right) 2D plane of the {^{15}N,^{13}C}-edited 4D HMQC−NOESY−HSQC spectrum taken at the H^N and N chemical shifts of Thr30. Peaks marked with an asterisk originate from a different plane. In the 4D plane, the overlapping resonances of Val29 H^{α} and Lys130 H^{α} at 5.38 and 5.37 ppm and $H^{\gamma 1}$ of Thr129 and $H^{\gamma 2}$ Val32 at 0.90 and 0.89 ppm, respectively (indicated by arrows), in the 3D slice could be resolved.

(Figure 1, right panel) corresponding to a slice in the 3D spectrum with given H^N and N shifts (left panel), the contributions of different aliphatic nuclei with degenerate chemical shifts can be detected. In Figure 1, the plane taken at the H^N and N chemical shifts of Thr30 leads to resolution of NOE peaks for H^{α} of Val29 and Lys130 at 5.38 and 5.37 ppm, respectively, as well as $H^{\gamma 1}$ of Thr129 and $H^{\gamma 2}$ Val32 at 0.90 and 0.89 ppm, respectively. Eight hundred eighty-five cross-peaks in the ^{15}N-edited 3D NOESY spectrum and 446 cross-peaks in the ^{13}C-edited 3D NOESY spectrum were assigned prior to the initial DYANA calculations. Structure calculations with this initial data set yielded structures with global rmsds of 3.49 and 2.45 Å for heavy and backbone atoms, respectively. The assignments were extended in cycles of structure calculations followed by new cross-peak assignments with the program ASNO. In later cycles of the structure calculations, 26 hydrogen bond constraints were included (see Materials and Methods). This procedure resulted in an additional 306 and 682 unambiguous NOE assignments for the ^{15}N-edited and the ^{13}C-edited 3D NOESY data sets, respectively.

Distance Geometry Calculations. A total of 1191 NOEs from the ^{15}N-edited NOESY spectrum and 1128 NOEs from the ^{13}C-edited NOESY spectra resulted in a total of 1658 meaningful distance constraints. Local conformational analysis using these NOE constraints together with 104 ^3J scalar coupling constants resulted in 335 torsion angle constraints (125 ϕ, 106 ψ, and 94 χ_1). Of the distance constraints, 242 were intraresidue, 458 were sequential, 298 were medium-range (limit of four residues), and 660 were long-range. Figure 2 shows the distribution of the distance constraints along the amino acid sequence. The final solution structures were then calculated by simulated annealing torsion angle dynamics using this data set. The lowest target function (tf_{min}) was 1.28 Å^2, and 48% of the 100 calculated conformers were found to display target functions within the acceptance criterion limit (tf_{cut}) defined by Güntert et al. (*31*) with $tf_{cut} = tf_{min} + (n_{res}0.02$ Å^2), with n_{res} giving the number of amino acid residues. Of the final 100 structures calculated, the 20 conformers with the lowest target function were chosen to represent the NMR solution structure and further analyzed. Table 1 summarizes the structural statistics. All 20 structures had target functions below 3 Å^2 (mean target function of 2.42 Å^2). On average, the structures display a maximum distance violation of 0.32 Å and torsion angle violations of 5.6°, which are an indication of good consistency with the experimental data. The conformational parameters of the

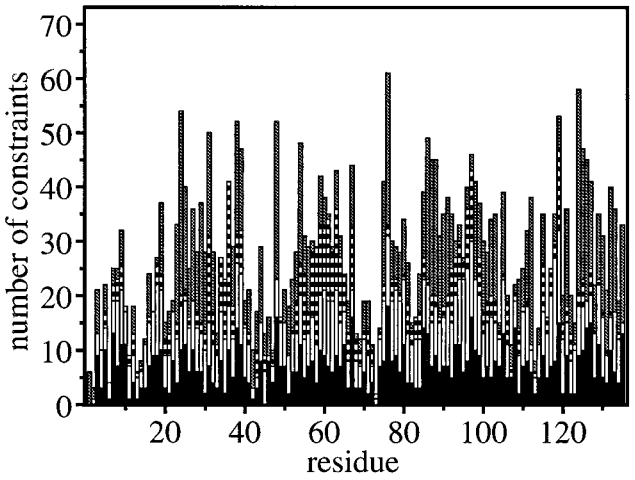

FIGURE 2: Number of NOE constraints per amino acid residue in the sequence of staphylokinase. The shading of the bars corresponds to the following constraints: black, intraresidual; white, sequential; hatched, medium-range; and gray, long-range.

Table 1: Structural Statistics for Staphylokinase

	average value ± standard deviation (range)
DYANA target function (Å^2)	2.42 ± 0.46 (1.28−2.97)
no. of residual violations	
NOE distance constraints, maximum (Å)	0.32 ± 0.05 (0.22−0.44)
NOE distance constraints, sum (Å)	9.30 ± 1.23 (6.7−11.1)
dihedral angle constraints, maximum (deg)	5.56 ± 2.16 (3.4−11.2)
dihedral angle constraints, sum (deg)	33.70 ± 8.34 (16.5−49.1)
mean AMBER energy (kcal/mol) of the 20 energy-minimized structures	390 ± 28 (338−449)
rmsds (Å) from the mean structure	**before/after energy minimization**
backbone atoms (residues 16−136)	0.87 ± 0.16/0.89 ± 0.17
all heavy atoms (residues 16−136)	1.36 ± 0.14/1.40 ± 0.14
backbone atoms (core[a])	0.72 ± 0.13/0.74 ± 0.14
all heavy atoms (core[a])	1.14 ± 0.12/1.17 ± 0.12

[a] The core region includes residues 20−71, 78−114, and 121−134, which covers the β-sheets, the α-helix, and the well-defined connecting loops of residues 20−23, 34−36, 40−46, 50−52, 80−86, 94−97, 105−110, and 121−123.

NMR solution structures were checked with the program PROCHECK (*37*). This showed that, over all 20 structures, 96% of the backbone angle combinations for non-Gly residues are within the allowed and 52.6% are in the most favored regions of the Ramachandran plots (*38*). Residues displaying a positive ϕ torsion angle due to strong intraresidual H^N-H^α NOEs, intermediate $^3J_{HNH\alpha}$ coupling constants, or a lack in distance or torsion angle restraints are mainly located in the regions displaying higher conformational mobility (residues 2−19, 43−46, and 74−76; see below) and the less well-defined loop of Asp115−Glu118.

For the superimposed structures, the rmsd over all backbone heavy atoms was calculated to be 1.02 ± 0.15 Å, while the all-heavy atom rmsd was 1.53 ± 0.17 Å. The N-terminal sequence (residues 1−19) is the least well-defined structural region, which is consistent with the observation that all amide H^N hydrogens of these residues exchanged rapidly with solvent (*11*). Superposition of residues 16−136 led to rmsd values for the atomic positions of 0.87 (backbone heavy atoms) and 1.36 Å (all heavy atoms). The mean of the potential energy for the 20 conformers after energy minimization was 390 kcal mol^{-1} with a strong negative van der Waals contribution of 1080 kcal mol^{-1} which is indicative of relaxed nonbonded interactions. The distribution of the backbone angular order parameters (AOPs) along the amino acid sequence shown in Figure 3 provides a further measure of the extent to which the present NMR data defines the 3D structure. Sixty-seven percent of the backbone angles ϕ and ψ exhibit angular order parameters of >0.9 (83 ϕ and 98 ψ), corresponding to angular fluctuations of less than 25° and to a well-defined backbone conformation (*39*). The backbone AOPs are low for the 20 N-terminal residues, for residues 34−36 and 115−117 in loops connecting β-strands, and in residues 70−78 between the end of the α-helix and the next β-strand. The side chains are less well-defined as indicated by the fluctuations in the AOPs of χ_1. Of 115 residues with meaningful χ_1 angles, i.e., excluding Gly, Ala, and Pro, 51 residues exhibited side chain AOPs of >0.9. The bulk of these were located in the α-helix and the β-strands.

Structural and Dynamical Features. The folded conformation of Sak (Figure 4) includes a central α-helix composed of residues Lys57−Thr71 which is positioned over an ensemble of five β-strands and flanked by a short, three-residue double-stranded β-sheet (residues 53−55 and 111−113). The five-stranded β-sheet ensemble consists of a parallel sheet involving residues Tyr24−Asp33 and Gly124−Glu134 associated with antiparallel strands (residues 37−39, 47−49, 78−80, 87−93, and 98−104). β-Sheet residues Tyr24−Asp33 are associated with two short β-strands, Asn37−Leu39 and Phe47−Ile49. The intervening residues, Leu40−Glu46, constitute a two-residue bulge which leads to formation of an irregular structure rather than a continuous β-strand. At the present level of structural refinement, the core of the Sak molecule comprising the α-helix, β-strands, and connecting loops (residues 20−71, 78−114, and 121−134) is well-defined with a backbone rmsd of 0.72 Å from the mean structure (Table 1). The N-terminal region (residues 1−19) and several of the loop regions (residues 72−77 and 115−120) as well as the C terminus (residues 135 and 136) correspond to solvent-exposed regions of the structure and exhibit a lower number of distance restraints

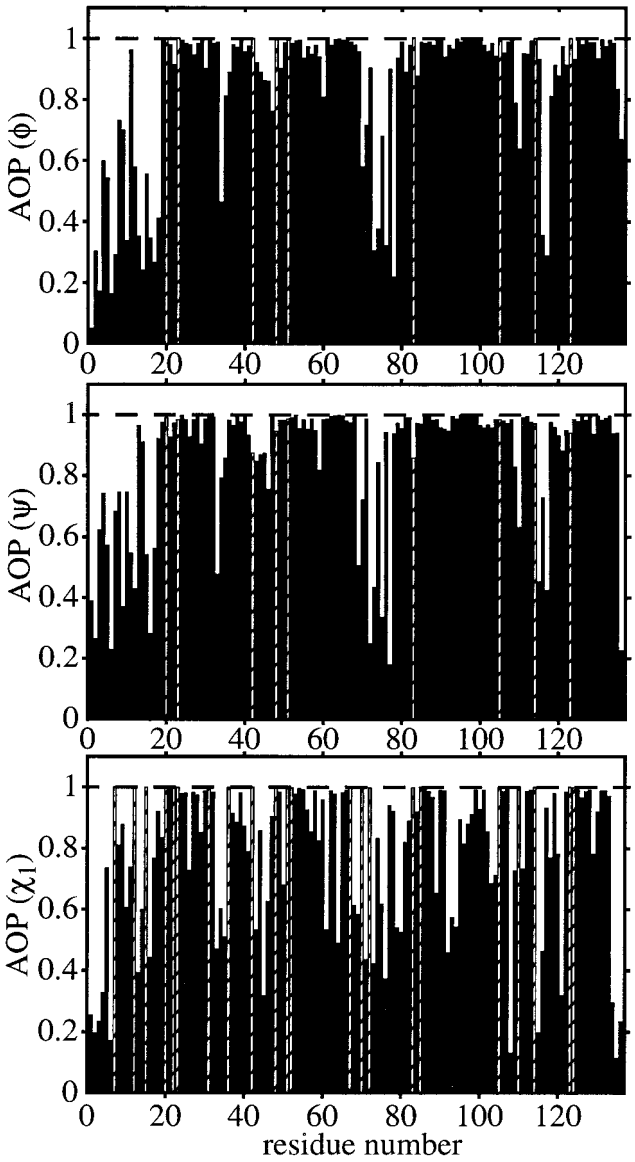

FIGURE 3: Angular order parameters (AOPs) for torsion angles ϕ, ψ, and χ_1 in the 20 best conformers of staphylokinase. Columns for proline residues are hatched. The positions of glycines and alanines are also hatched in the χ_1 plot.

as well as fast exchange of their amide protons with solvent water. The α-helix, which lies essentially perpendicular to the five-stranded β-sheet, is amphiphilic with the hydrophilic and acidic residues Glu58, Glu61, Glu65, and Asp69 mainly located on the same side of the α-helix. In the α-helix, the side chains of aromatic residues Tyr62, Tyr63, and Trp66 as well as Lys59 point away from the β-sheet, are solvent-exposed, and show relatively few NOE contacts. The 3D structure is fully consistent with the hydrogen bonding patterns and secondary structure determined earlier (*11*). It also shows hydrogen bonds for residues in irregular regions of the 3D structure (e.g., NH of Ile106) which were previously observed to show slow exchange with solvent water. Following the SCOP (*40*) and CATH classifications (*41*), Sak belongs to the β-grasp fold family or the Alpha-Beta protein class with a roll architecture, respectively.

A visual inspection of the recent X-ray structure (*12*) shows good similarity of the global fold for residues 16−136. The molecule studied by X-ray crystallography lacked residues 1−10 due to proteolytic degradation, and residues

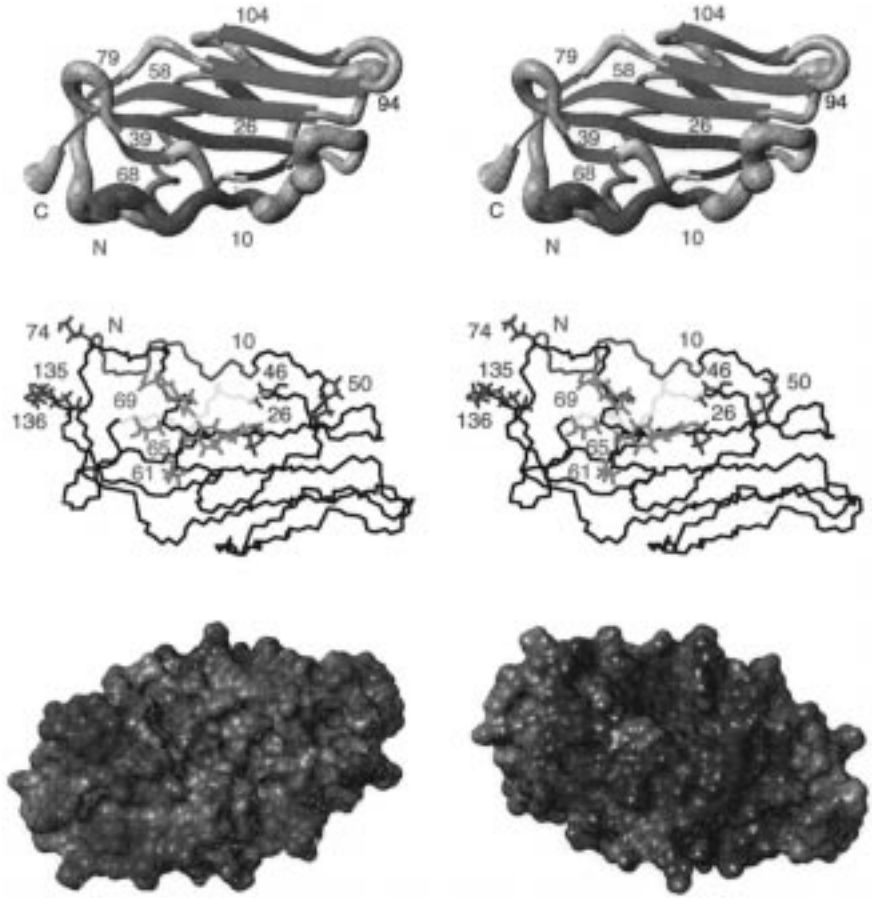

FIGURE 4: (A, top) Stereoview of a mixed ribbon and tube diagram of the mean structure of the 20 best conformers of staphylokinase. The color scheme includes red for the α-helix (residues 57−71), cyan for β-sheets, green for residues 1−10, yellow for residues 40−46, and gray for all others. The thickness of the tube in the nonsheet regions represents the mean of the global displacement among the 20 solution structures. The tube diameters in the overlapping elements at the ends of the β-sheet ribbons are indicative of the β-sheet displacements. (B, middle) Stereoview of the Sak backbone for the conformer closest to the mean structure. The orientation corresponds to Figure 4A rotated by 180° about a horizontal axis in the plane of the paper. The side chains of residues M26, E46, K50, K74, K135, and K136 are blue. Aromatic (Y62, Y63, and W66) and acidic residues (E61, E65, and D69) in the α-helix are red. The N terminus (residues 1−10) and the backbone in the bulge region (residues 40−46) are green and yellow, respectively. (C, bottom) Representations of the hydrophilicity of the surface of staphylokinase in the orientation of panel A (left) and panel B (right). The color scale is hydrophilic to hydrophobic in the order blue to gray to green to brown.

11−15 were not observed due to structural disorder; however, it was proposed that residues 1−15 would extend into the solvent and have a minimal effect on the overall structure of Sak (*12*). Although amino acid residues Ser1−Glu19 of Sak show some degree of conformational heterogeneity in the NMR solution structure and may be partly flexible (see below), we observe that the N-terminal residues fold back onto the core of the Sak structure. This appears to involve a loose, irregular association since a relatively limited number of NOEs were observed, including those between residues 2−40, 73, 75, and 76; 3−39 and 72; 4−40, 43, 44, 68, 71, 72, and 76; 6−44 and 71; 8−41, 42, and 43; 9−44 and 45; 10−43, 44, 45, 46, and 47, as well as a further 16 NOEs from residues 11 to 19 to other parts of the protein structure. Rapid exchange of backbone amide hydrogens was observed for residues 1−22.

To assess possible flexibility in the backbone of Sak, ^{15}N−{^{1}H} NOEs were determined for 114 of the 127 backbone amides (Figure 5). For residues 4−19, all observable nitrogens showed NOE values below −0.4. This corresponds to low angular order parameters for the ϕ and ψ backbone torsion angles (Figure 3) and to large backbone rmsd values (Figure 5) for these residues in the calculated staphylokinase structures. Taken together, the above observations indicate that the N-terminal region shows the highest degree of conformational variability in the solution structure of Sak. When NOE values of −0.4 are taken as an operative indication of the regions with more variability, only three other residues exceed this threshold (Figure 5). Residue His43 is positioned in the bulge between short β-strands Asn37−Leu39 and Phe47−Ile49, and Tyr73 and Glu75 reside in a loop following the α-helix. All of these residues exhibit fast exchange of amide hydrogens with solvent. The amide hydrogens of Tyr44 and Lys74 have not been observed in any of the NMR spectra, presumably as a consequence of rapid exchange with solvent. Between Ala72 and Val78, a decrease in the angular order parameters for the 20 best conformers and large local rmsds are observed. This suggests that the loop (residues 72−76) joining the α-helix to the subsequent β-sheet is a further region of larger conformational variability in the Sak molecule. Weak heteronuclear NOEs and low values for the rmsd are observed for residues located in the regular secondary structural elements (Figure 5).

Structural Interpretation of Biochemical Data. The ability of Sak to alter the proteolytic specificity of plasmin and

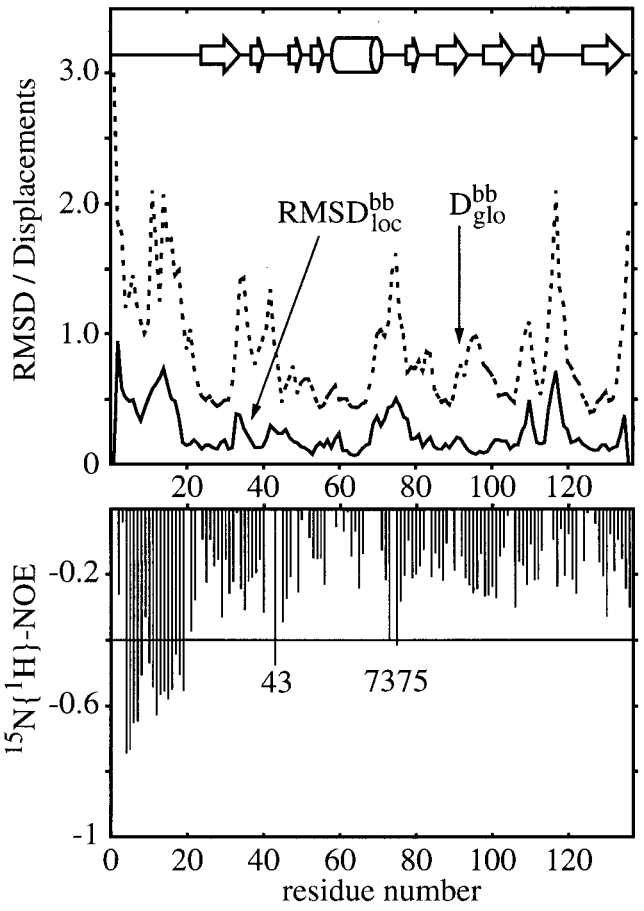

FIGURE 5: (Top) Mean local rmsd values at residue i (RMSD$^{bb}_{loc}$) for the backbone heavy atoms of residues $i - 1$, i, and $i + 1$ following local superposition of sequential tripeptides. Mean global backbone displacements per residue (D^{bb}_{glo}) relative to the mean structure following a global superposition of the core. Residues involved in β-sheets (arrows) and the α-helix (cylinder) are indicated at the top. (Bottom) ^{15}N−{^{1}H} NOEs for staphylokinase. With the exception of the N-terminal region (residues 1−19), residues with ^{15}N−{^{1}H} NOEs of less than −0.4 (see the text) are indicated.

thereby to lead to plasminogen activation is a fascinating property. The activation process appears to involve several characteristics, including both protein−protein recognition and complex formation as well as proteolytic hydrolysis of Sak itself. While the N-terminal region of Sak must be located near the active site of plasmin to allow the initial cleavage of Sak at Lys10, there need to be other interactions which maintain the protein−protein complex, but lead to a free active site of plasmin with altered proteolytic activity once residues 1−10 have been removed from Sak.

The site of the initial proteolytic cleavage of Sak at Lys10 lies on the surface of the molecule and is highly exposed to solvent (Figure 4A). The loose association of residues 1−15 with the core of Sak observed in this study may facilitate the initial proteolytic step during plasminogen activation, and it appears that this cleavage step leads to some rearrangement of the Sak structure. From the NMR structure, it is apparent that proteolytic cleavage of residues 1−10 will result in increased exposure to solvent of several regions of the core of the Sak structure. This is especially true for the bulge region constituted by residues 40−46, which show an increase of solvent-exposed surface from 9.5 to 22.5% upon removal of residues 1−10 and to 26.5% upon removal of residues 1−15 from the NMR structure. Exactly the cleaved residues Ser1−Lys10 are involved in interactions with residues Leu40−Glu46; e.g., NOEs are observed from Tyr44 and His43 to Phe4, Lys6, Lys8, Tyr9, and Lys10. Given the close proximity to the initial cleavage site at Lys10, it is interesting that this bulge region shows conformational differences between the X-ray and solution structures. In the X-ray structure, close van der Waals contacts between Met26 and Tyr44 were observed (*12*). These spatial proximities are not observed in the solution structure, and NOEs are instead observed from Tyr44 to Val45 and Glu46 and from the Met26 methyl group to the side chains of residues Asn126 and Ile128, which requires a rearrangement of the backbone in the bulge region relative to the X-ray structure. On the basis of the NMR solution structure of Sak residues 1−136, i.e., the structure prior to the initial activation step, and the crystal structure for Sak residues 11−136, i.e., the structure following the initial activation step, it seems that a "conformational switch" involving a change in the structure of residues 40−46 of Sak may be involved in the initial activation of plasminogen by staphylokinase. The pinning of the ends of this bulge via the participation of residues 37−39 and 47−49 in short β-sheets together with the indication from the present relaxation measurements that the His43 residue located in the center of the bulge may be conformationally labile suggests that residues 40−46 might be poised for interaction with plasminogen in the activation process. These residues are clearly close to the active site of plasmin and may play a role in altering the proteolytic specificity of plasmin.

To achieve activation and modulation of the proteolytic specificity, plasmin and Sak form a complex (*42*) which is known to involve quite strong binding (K_D = 50 nM; *43*) and is therefore suggestive of a fairly extensive protein−protein interaction. There is substantial biochemical information which can be used to assess which regions of the staphylokinase structure may be important for binding of plasminogen. Studies on the thermostability of the three known wild-type staphylokinases indicated that the substitutions S34G and G36R produced only small differences in activation (*44*), suggesting that the loop of residues 34−36 is not important for binding or activation. By deletion mutagenesis, it was found that both C-terminal residues were required for activation, but Lys135 and Lys136 could be replaced by alanine (*45*). Elongation of the C terminus by seven residues did not alter plasminogen activation. Lys135 and Lys136 show steric interactions with the flexible loop around Lys74 (Figures 4 and 5) and one of the β-strands near Ser34. It is also interesting to note that attempts to reengineer Sak to achieve reduced immunogenicity and thereby improve its therapeutic properties (reviewed in ref *2*) have shown that mutation of Lys74 to Ala reduces antibody formation in human patients without alteration of specific activity or thrombolytic potency (*46*).

The study by Gase et al. (*45*) also showed that SakΔN10 (comprising residues 11−136) is adequate for completion of the subsequent steps in plasminogen activation. Furthermore, mutants involving additional N-terminal truncation of SakΔN10 for which positively charged residues (Lys) were retained at the new N terminus [e.g., SakΔN15(S16K)] continued to show plasminogen activation. Substitution of clusters of charged amino acid residues by alanine led to

the identification of only three clusters in which the changes almost completely abolished the activity of Sak (*47*). One of these clusters, centered around the site of initial proteolytic cleavage at Lys10−Lys11, was investigated in detail. It was shown that the mutant SakSTAR (K11A/D13A/D14A) retained intact binding to plasminogen (*47*), but the cleavage of the Lys10−Lys11 bond is a prerequisite for activation of plasminogen and thereby is the trigger of the fibrin specificity of Sak (*10*). The other two important mutation sites identified by the charged amino acids to alanine scan, i.e., mutants SakSTAR (E46A/K50A) and SakSTAR (E65A/D69A), led to largely inactive mutants with impairment both of plasminogen binding and of subsequent generation of the plasmin active site. The solution structure shows that the first of these mutation sites is shielded from solvent exposure by the NH_2-terminal region of staphylokinase. All of these mutations are located largely in the upper region of the Sak structure (Figure 4B). In this context, it is interesting that the structure of Sak shows a strong asymmetry in hydrophilic and hydrophobic surfaces (Figure 4C; *48*) which is in part due to an unusual distribution of amino acids in the α-helix. Residues Ile60, Val64, Ala67, Leu68, and Thr71 are positioned between the helix backbone and the underlying β-sheets. The acidic side chains of Glu61, Glu65, and Asp69 form a charged flank of the helix, while aromatic residues Tyr62, Tyr63, and Trp66 are all highly exposed to solvent on one edge of the α-helix (Figure 4B). These aromatic residues, as well as Tyr73 and Phe76, contribute to the most hydrophobic region of the Sak surface shown in Figure 4C. The asymmetry in the hydrophobicity of the surface of Sak probably accounts for the ability to purify this protein by hydrophobic interaction chromatography and may well be important for recognition of plasmin(ogen) since mutations in this region of the structure, e.g., SakSTAR (E65A/D69A), lead to impaired binding.

CONCLUSION

In short, the sequence positions identified as functionally important by biochemical and mutational studies are all located in the general proximity of the N-terminal residues, the bulge region of residues 40−46, and the helix (Figure 4B). Sensitivity to structural variations in this region of the molecule is also consistent with the results of an NMR study of the M26A mutant (D. Fandrei and O. Ohlenschläger, work in progress) which shows that the replacement of methionine by alanine leads to a change in β-sheet contacts with a concomitant loss of the ability to activate plasminogen (*49*). It seems probable that this region (Figure 4B) of the Sak molecule is involved in protein−protein contacts necessary for formation of the complex with plasmin(ogen) and that conformational rearrangements, especially near the bulge region of residues 40−46 and the new N terminus at residue Lys11, may well be necessary for achieving the ability of Sak to alter the proteolytic specificity of plasmin. To further clarify the mechanisms by which Sak activates plasminogen, further structure−function studies of mutant staphylokinase molecules are underway in our laboratories.

ACKNOWLEDGMENT

We thank Mr. J. Leppert and Mr. M. Semm for excellent technical assistance.

SUPPORTING INFORMATION AVAILABLE

Two tables showing (1) the acquisition and processing parameters for the NMR experiments and (2) the chemical shifts for staphylokinase at 27 °C (7 pages). Ordering information is given on any current masthead page.

REFERENCES

1. Collen, D., and Van de Werf, F. (1993) *Circulation 87*, 1850−1853.
2. Collen, D. (1998) *Nat. Med. 4*, 279−284.
3. Vanderschueren, S., Stockx, L., Wilms, G., Lacroix, H., Verhaeghe, R., Vermylen, J., and Collen, D. (1995) *Circulation 92*, 2050−2056.
4. Collen, D., Schlott, B., Engelbourghs, Y., Van Hoef, B., Hartmann, M., Lijnen, H. R., and Behnke, D. (1993) *J. Biol. Chem. 268*, 8284−8289.
5. Brockway, W. J., and Castellino, F. J. (1974) *Biochemistry 13*, 2063−2070.
6. Collen, D. (1985) *Circulation 72*, 18−20.
7. Zamarron, C., Lijnen, H. R., Van Hoef, B., and Collen, D. (1984) *Thromb. Haemostasis 52*, 19−23.
8. Lijnen, H. R., Van Hoef, B., De Cock, F., Okada, K., Ueshima, S., Matsuo, O., and Collen, D. (1991) *J. Biol. Chem. 266*, 11826−11832.
9. Silence, K., Collen, D., and Lijnen, H. R. (1993) *J. Biol. Chem. 268*, 9811−9816.
10. Schlott, B., Gührs, K.-H., Hartmann, M., Röcker, A., and Collen, D. (1997) *J. Biol. Chem. 272*, 6067−6072.
11. Ohlenschläger, O., Ramachandran, R., Flemming, J., Gührs, K.-H., Schlott, B., and Brown, L. R. (1997) *J. Biomol. NMR 9*, 273−286.
12. Rabijns, A., De Bondt, H. L., and De Ranter, C. (1997) *Nat. Struct. Biol. 4*, 357−360.
13. Schlott, B., Hartmann, M., Gührs, K.-H., Birch-Hirschfeld, E., Pohl, H.-D., Vanderschueren, S. B., Van De Werf, F., Michoel, A., Collen, D., and Behnke, D. (1994) *BioTechnology 12*, 185−189.
14. States, D. J., Haberkorn, R. A., and Ruben, D. J. (1982) *J. Magn. Reson. 48*, 286−292.
15. Piotto, M., Saudek, V., and Sklenar, V. (1992) *J. Biomol. NMR 2*, 661−665.
16. Shaka, A. J., Barker, P. B., and Freeman, R. (1985) *J. Magn. Reson. 64*, 547−552.
17. Fujiwara, T., Anai, T., Kurihara, N., and Nagayama, K. (1993) *J. Magn. Reson. A104*, 103−105.
18. Shaka, A. J., Lee, C. J., and Pines, A. (1988) *J. Magn. Reson. 77*, 274−293.
19. Bartels, C., Xia, T., Billeter, M., Güntert, P., and Wüthrich, K. (1995) *J. Biomol. NMR 6*, 1−10.
20. Wishart, D., and Sykes B. D. (1994) *J. Biomol. NMR 4*, 171−180.
21. Fesik, S. W., and Zuiderweg, E. R. P. (1988) *J. Magn. Reson. 78*, 588−593.
22. Zuiderweg, E. R. P., and Fesik, S. W. (1989) *Biochemistry 28*, 2387−2391.
23. Muhandiram, D. R., Guang, Y. X., and Kay, L. (1993) *J. Biomol. NMR 3*, 463−470.
24. Vuister, G. W., Clore, G. M., Gronenborn, A. M., Powers, R., Garrett, D. G., Tschudin, R., and Bax, A. (1993) *J. Magn. Reson. B101*, 210−213.
25. McCoy, M. A., and Müller, L. (1993) *J. Magn. Reson. A101*, 122−130.
26. Delaglio, F., Grzesiek, S., Vuister, G. W., Zhu, G., Pfeifer, J., and Bax, A. (1995) *J. Biomol. NMR 6*, 277−293.
27. Vuister, G. W., and Bax, A. (1993) *J. Am. Chem. Soc. 115*, 7772−7777.
28. Montelione, G. T., Winkler, M. E., Rauenbuehler, P., and Wagner, G. (1989) *J. Magn. Reson. 82*, 198−204.
29. Glaser, R. W. (1997) http://www.mol.biol.ethz.ch/wuthrich/software/spscan/.
30. Kay, L. E., Torchia, D. A., and Bax, A. (1989) *Biochemistry 28*, 8972−8979.

31. Güntert, P., Mumenthaler, C., and Wüthrich, K. (1997) *J. Mol. Biol. 273*, 283−298.
32. Güntert, P., Berndt, K. D., and Wüthrich, K. (1993) *J. Biomol. NMR 3*, 601−606.
33. Pearlman, D. A., Case, D. A., Caldwell, J. W., Ross, W. S., Cheatham, T. E., III, Ferguson, D. M., Seibel, G. L., Chandra Singh, U., Weiner, P. K., and Kollman, P. A. (1995) *AMBER 4.1*, University of California, San Francisco, CA.
34. Cornell, W. D., Cieplak, P., Bayly, C. I., Gould, I. R., Merz, K. M., Jr., Ferguson, D. M., Spellmeyer, D. C., Fox, T., Caldwell, J. W., and Kollman, P. A. (1995) *J. Am. Chem. Soc. 117*, 5179−5197.
35. Guenot, J. M., and Kollman, P. A. (1992) *Protein Sci. 1*, 1185−1205.
36. Koradi, R., Billeter, M., and Wüthrich, K. (1996) *J. Mol. Graphics 14*, 51−55.
37. Laskowski, R. A., McArthur, M. W., Moss, D. S., and Thornton, J. M. (1993) *J. Appl. Crystallogr. 26*, 283−291.
38. Morris, A. L., MacArthur, M. W., Hutchinson, E. G., and Thornton, J. M. (1992) *Proteins 12*, 345−364.
39. Hyberts, S. G., Goldberg, M. S., Havel, T. F., and Wagner, G. (1992) *Protein Sci. 1*, 736−751.
40. Murzin, A. G., Brenner, S. E., Hubbard, T., and Chothia, C. (1995) *J. Mol. Biol. 247*, 536−540.
41. Orengo, C. A., Michie, A. D., Jones, S., Jones, D. T., Swindells, M. B., and Thornton, J. M. (1997) *Structure 5*, 1093−1108.
42. Lijnen, H. R., and Collen, D. (1996) *Fibrinolysis 10*, 119−126.
43. Lijnen, H. R., De Cock, F., Van Hoef, B., Schlott, B., and Collen, D. (1994) *Eur. J. Biochem. 224*, 143−149.
44. Gase, A., Birch-Hirschfeld, E., Gührs, K.-H., Hartmann, M., Vettermann, S., Damaschun, G., Damaschun, H., Gast, K., Misselwitz, R., Zirwer, D., Collen, D., and Schlott, B. (1994) *Eur. J. Biochem. 223*, 303−308.
45. Gase, A., Hartmann, M., Gührs, K.-H., Röcker, A., Collen, D., Behnke, D., and Schlott, B. (1996) *Thromb. Haemostasis 76*, 755−760.
46. Collen, D., Stockx, L., Lacroix, H., and Vanderschueren, S. (1997) *Circulation 95*, 463−472.
47. Silence, K., Hartmann, M., Gührs, K.-H., Gase, A., Schlott, B., Collen, D., and Lijnen H. R. (1995) *J. Biol. Chem. 270*, 27192−27198.
48. Heiden, W., Moeckel, G., and Brickmann, J. (1993) *J. Comput.-Aided Mol. Des. 7*, 503−514.
49. Schlott, B., Hartmann, M., Gührs, K.-H., Birch-Hirschfeld, E., Gase, A., Vettermann, S., Collen, D., and Lijnen, H. R. (1994) *Biochim. Biophys. Acta 1204*, 235−242.

BI980673I